Uptake of Breathable Nano- and Micro-Sized Polystyrene Particles: Comparison of Virgin and Oxidised nPS/mPS in Human Alveolar Cells

Antonio Laganà , Giuseppa Visalli , Alessio Facciolà , Consuelo Celesti , Daniela Iannazzo , Angela Di Pietro *

Posted Date: 11 July 2023

doi: 10.20944/preprints202307.0678.v1

Keywords: environmental wear; uptake; cytotoxicity; ROS overproduction; mitochondrial dysfunction

Article

Uptake of Breathable Nano- and Micro-Sized Polystyrene Particles: Comparison of Virgin and Oxidised nPS/mPS in Human Alveolar Cells

Antonio Laganà [1,2], Giuseppa Visalli [1], Alessio Facciolà [1], Consuelo Celesti [3], Daniela Iannazzo [3] and Angela Di Pietro [1*]

[1] Department of Biomedical and Dental Sciences and Morphofunctional Imaging, University of Messina, 98125 Messina, Italy; antonio.lagana1@studenti.unime.it; giuseppa.visalli@unime.com; alessio.facciola@unime.it; angela.dipietro@unime.it

[2] Istituto Clinico Polispecialistico C.O.T., Cure Ortopediche Traumatologiche s.p.a., 98124, Messina, Itay; antonio.lagana1@studenti.unime.it;

[3] Department of Electronic Engineering, Industrial Chemistry and Engineering, University of Messina, 98125 Messina, Italy; consuelo.celesti@unime.it; diannazzo@unime.it

* Correspondence: angela.dipietro@unime.it;

Abstract: Airborne micro- and nanoplastics are widely spread and pose a risk to human health. The effects of virgin (v) and home oxidised (ox) nano- and micropolystyrene (nPS/mPS) (0.1 and 1 μm) were studied on the human alveolar cells (A549). Ox-nPS/mPS, simulating photoaging, allowed effects due to environmental wear to be assessed. Cellular uptake was quantified using FITC-functionalised nPS/mPS, while cytotoxicity, changes in the acidic compartment, ROS production, mitochondrial function and DNA damage were assessed to study the effects of internalised v- and ox-nPS/mPS. The uptake was dose-dependent and very fast, since, at the lowest dose, 20.8% and 21.8% of nPS and mPS, respectively, were internalised after 1 h. Compared to v-, significant ROS increases, DNA damage and mitochondrial impairment were observed after exposure to ox-nPS/mPS. The enhancement of effects due to environmental aging processes highlighted the true potential impact on human health of these airborne pollutants.

Keywords: environmental wear; uptake; cytotoxicity; ROS overproduction; mitochondrial dysfunction

1. Introduction

Plastics, due to their malleability, high versatility and low cost, are currently widely used; their production is only slightly lower than that of concrete and steel. Low- and high-density polyethylene (PE), polypropylene (PP), polystyrene (PS), polyethylene terephthalate (PET), polyurethane (PUR), polycarbonate (PC) and polyvinyl chloride (PVC) are the most produced plastics due to their characteristics [1]. Despite the remarkable durability, around 50% of the total mass of currently manufactured plastics is disposable. This aspect has greatly increased their presence in different environmental matrices, where improperly disposed plastic waste undergoes a slow and partial physical, chemical and even biological degradation. Due to abiotic factors, such as the mechanical action of wind and wave motions and prolonged exposure to ultraviolet (UV) light (photo-oxidation), as well as by biotic factors (degradative microbiological processes), the fragmentation of plastic waste produces secondary microplastics (<5 mm) and, following further fragmentation, secondary nanoplastics with a diameter ≤0.1 μm [2]. In addition to these particles, primary microplastics and nanoplastics, which are intentionally and directly produced on a micro- and nanoscale as constituents of specific products, also contribute to plastic pollution [3]. Micro- and nanoplastics are persistent in the environment and can interact very easily with biological systems [4,5]. Indeed, they have been found in sediment [6], soil [7], seawater [8], high mountain lake ecosystems [9] and air [10], but also in many foods and beverages like shellfish, cooking salt, drinking water and beer [11]. Moreover, due to their hydrophobic nature, micro- and nanoplastics are highly bioavailable and are able to

 doi:10.20944/preprints202307.0678.v1

bioaccumulate, as confirmed by their presence in several organisms along the trophic scale, attesting to their biomagnification [12,13].

Humans are inevitably exposed to micro- and nanoplastics, mainly via ingestion and inhalation, while exposure by skin contact causes less concern [14–19]. Some very recent studies have verified the presence of microplastics in different body regions as well as their faecal excretion [20–24].

Airborne micro- and nanoplastics are derived from a variety of sources, including synthetic fibres, waste disposal products, incinerators, particles used in agriculture (such as PS peat) and sewage sludge used as fertiliser, as well as road traffic [10,25–27]. In particular, tyre wear particles (TWPs) and brake wear particles (BWPs) are formed by complex mixtures of metal and mainly microplastics. It has been estimated that in ambient air around 4% and 11% of the respirable (fine) and inhalable (coarse) PM, respectively, are formed by micro- and nanoplastics derived by TWPs and BWPs only [28].

In addition to ambient air (outdoor), exposure to airborne micro- and nanoplastics also occurs in indoor environments, where higher concentrations are present due to several sources, such as synthetic textile fibres, upholstery and furnishing objects or building materials, which release plastic particles after wearing down [29]. Indoor exposure to airborne micro- and nanoplastics appears to be highly relevant considering the lower dilution volumes and the time spent in indoor environments (on average 70–90% of our life).

We currently know a lot about the mechanisms responsible for the pathogenesis of airborne micro- and nanoparticulate matter (fine and ultrafine PM), as well as metal- and carbon-based engineered nanoparticles [30–32]. The ≤2.5 μm particles can overcome muco-ciliary clearance and reach the alveolar surface, wherein nanoparticles can bypass alveolar clearance, based on the phagocytic activity of macrophages. They easily cross the pulmonary epithelial barrier and enter the bloodstream, from where they are distributed to the various anatomical regions [33]. For micro- and nanoparticles, the number of surface atoms per unit mass is increased by several orders of magnitude, greatly enhancing the surface area for chemical reactions, while charge and polarity are fundamental in regulating cellular uptake and biological effects [34]. The pathogenesis of respirable micro- and nanoplastics is poorly known, but it can be assumed that the trigger is determined by intense oxidative stress, which causes lipid peroxidation, protein and DNA damages, mitochondrial dysfunction and inflammation in response to tissue damage [35].

The aim of this in vitro study was to investigate in human alveolar epithelial cells (A549 cell line) the uptake and the cytotoxic effects of polystyrene nanoplastics (nPS) and microplastics (mPS) with diameters of 0.1 and 1 μm, respectively. As the largest share of environmental nPS/mPS that humans inevitably inhale are the secondary ones, subjected to a long wear process (including photo-oxidation), for a more realistic assessment of biological effects, we examined in-home oxidised nPS/mPS, comparing the effects with virgin ones.

This was in order to determine how much the changes undergone in the environment, such as the presence on the surface of functional groups, enhances the reactivity of the particles, thus increasing the hazard for the exposed subjects.

2. Materials and Methods

2.1. Exposure conditions and cell models

Virgin nPS (average size 100 nm) and mPS (average size 1 μm) were purchased from Sigma-Merck (Milan, Italy; code: BCC8557 and BCC9279). The choice of diameters was based on the evidence that both mPS and nPS are part of the respirable fraction of inhalable particulate matter (≤2.5 μm).

mPS/nPS oxidation was performed by the method reported by Mielczarski et al. (2011) [36]. Briefly, to allow the presence of carboxyl, alkoxyl and hydroxyl groups on the particle surface, aliquots of stock suspensions in phosphate buffered saline (PBS, 1:10 ratio) were treated at 80°C for 2 h. The suspensions were characterised by Fourier-Transform Infrared (FT-IR) spectrometry, dynamic light-scattering (DLS), scanning electron microscopy (SEM) and UV-Vis spectrophotometry. As

 doi:10.20944/preprints202307.0678.v1

previously reported [37], dynamic light- scattering DLS analyses and SEM observations confirmed the same average size of the functionalised microplastics, suggesting that oxidation occurred only at the surface of the particles and it did not cause their aggregation, either in PBS and in cell medium suspensions UV-Vis and FTIR spectra highlighted the presence of oxygen functionalities, such as carbonyl and phenol groups. To quantify spectrofluorometrically the cellular uptake, these functionalised particles were covalently bound to fluorescein isothiocyanate (FITC). Specifically, the conjugation was performed using 1-ethyl-3-(3-dimethylaminopropyl) carbodiimide (EDC) and hydroxybenzotriazole (HOBt) as coupling reagents, and a polyethylene glycol (PEG) linker. This had two amino groups, one of which was previously bound to FITC, while the other was bound to functionalised particles (i.e. ox-mPS- and ox-nPS). The reaction steps, as well as the purification steps, were reported in detail in a previous study [37]. The complexes were then analysed by FTIR spectroscopy while the photoluminescence (PL) properties were investigated by dynamic light scattering (DLS) [37].

The cellular uptake and the biological effects of virgin (v-) and oxidised (ox-) mPS/nPS suspensions were assessed in the human alveolar cell line A549 (ATCC-CCL-185Tm), which is the model of choice for in vitro studies of airborne pollutants. The cells were cultured in F-12K medium (Gibco™ 21127022) supplemented with 2 mM of L-glutamine, 10% of inactivated foetal bovine serum (FBS), and 1% penicillin/streptomycin/amphotericin, at 37°C in a 5% CO_2/95% air humidified atmosphere. For all experiments, the exposure treatment for times and doses established in the experimental protocol was performed in semiconfluent monolayers (75%) grown for 24–36h and incubated with nPS/mPS suspensions that were set up in cell medium containing 2% FBS (maintenance cell medium). Although the presence of proteins could partially neutralise the effect of the particles due to the so-called "protein corona", we believe that this protocol best simulates what actually happens. The corona effect hinders the intake due to their increased bulk and the loss of hydrophobicity which is known to promote the interaction of particles with cell membranes [38]. Moreover, the protocol meant that exposure to xenobiotics occurred in physiological conditions and not in cells which, kept in suboptimal conditions, could lead to an overestimation of the effects. Cells treated with PBS without mPs/nPSwere used as a negative control while cells treated with suitable compounds were used as positive controls.

2.2. Cellular uptake of mPS/nPS

The stock suspensions of nPS-FITC/mPS-FITC (80 μg mL^{-1}) were diluted in culture medium and added (100 μl/well), in the range of 1.25–20 μg/well, to A549 cells that had been grown for 24h in 96-well microplates (final density 4 × 10^4 cells/well). After 0.5, 1, 3 and 24h, fluorometric reading was carried out at the excitation and emission wavelengths of 485 nm and 535 nm, respectively, by using a microplate reader (Tecan Italia, Milan, Italy). After recording the emission values in each well, the medium was removed, the monolayer was washed repeatedly with PBS, to remove uninternalized particles, and emission values were recorded to measure the percentage uptake (i.e., intracellular mPS-FITC/nPS-FITC). Moreover, A549 monolayers grown in chamber slides were examined with confocal laser scanning microscopy (CLSM) using the Leica TCS SP2 instrument (Leica Microsystems, Wetzlar, Germany), with Leica Confocal software (version 2.0) used to process the images, which were acquired in both fluorescence and phase contrast. Leica DM IRB fluorescence microscope (Leica Microsystems) was used to select the optical fields.

2.3. Viability assays

In A549 cells, v-and ox mPS/nPS-induced cytotoxicity was evaluated by using the colorimetric MTT assay, based on the reduction of 3,(4,5-dimethiazol-2)-2,5-difeniltetrazolium bromide, catalysed by cellular NAD(P)H-dependent dehydrogenases. Briefly, after verifying the absence of particle interference in the spectrophotometric detection of cell viability, the assay was performed in cells cultured for 24h in 96-well microplates, to which the appropriate volume of stock suspensions in PBS (10 mg mL^{-1}) was added in the medium. The tested concentrations ranged from 12.5 to 200 μg mL^{-1}. Dimethyl sulphoxide (DMSO, 10%) was used as a positive control and eight different wells were

 doi:10.20944/preprints202307.0678.v1

treated for each dilution. After following our standardised protocol [37], the enzymatic activity was quantified by spectrophotometric measurement at 540 nm, using a microplate reader (Tecan Italia). The optical density (OD) values obtained for each sample were compared to the mean OD of the negative control, which was arbitrarily considered corresponding to 100% viability

2.4. Assessment of the cellular acidic compartment

Changes in the endocytic apparatus (late endosomes and lysosomes), due to the uptake of virgin and oxidised mPS/nPS, were examined by employing metachromatic fluorophore acridine orange (AO), which is captured by protons and collected in the acidic compartment. Here, the highly concentrated probe will emit red fluorescence, while it will release green fluorescence in the cytosol and nucleus, where AO scarcely accumulates. The loss of red fluorescence is indicative of acidic compartment damage [39]. The analyses were performed in semi-confluent A549 monolayers grown in chamber slides and treated for 3 and 24 h at 37°C with mPS/nPS suspensions (100 μg mL^{-1}). After removing the medium and washing repeatedly with PBS, AO solution (5 μg mL^{-1}) was added and CLSM was used to assess the endocytic apparatus and other morphological changes which were nPS/mPS-induced. To quantify the acid compartment, the image processing program Image J (imagej.nih.gov/ij/index.html) was used to calculate the cellular area which emitted red fluorescence. These values were expressed as % referred to the total area of each cell and at least 100 cells were analysed for each slide.

2.5. Evaluation of ROS production

To test the pro-oxidant effect of v- and ox-mPS/nPS, ROS were measured by using the 2',7'-dichlorofluorescein-diacetate (DCF-DA) probe (Merck Life Science S.r.l.). After crossing cell membranes by passive diffusion, the reagent is hydrolysed rapidly by cellular esterases to 2',7'-dichlorofluorescein (DCFH). This non-fluorescent compound is oxidised in the presence of ROS, forming the highly fluorescent molecule 2',7'-dichlorofluorescein (DCF). Briefly, after repeated washing with PBS, sub-confluent A549 monolayers (80%) in 96-well microplates were loaded with the probe solution (1 μM) prepared in PBS containing 10 mM of D-glucose (pH 7.4) and were incubated at 37°C for 30 min [40]. After washing in PBS to remove the non-internalised probe, cells were treated with v- and ox-mPS/nPS suspensions (in the range of 25-200 μg mL^{-1}). The fluorometric reading was carried out in the interval 0.5–24h by using a microplate reader (Tecan Italia) at the excitation and emission wavelengths of 485 and 535 nm, respectively. ROS production was calculated as the percentage change (Δ%) compared with control cells.

2.6. Mitochondrial transmebrane potential

To assess mitochondrial impairment induced by v- and ox-nPS/mPS, we measured transmembrane potential by the incorporation of the fluorescent probe rhodamine 123 (R123) (Invitrogen Molecular Probes). The chemical properties of the cationic fluorochrome R123 allow mitochondrial membrane crossing and storage in the matrix only in functional mitochondria that possess a transmembrane potential (ΔΨm), which is indicative of an active proton gradient maintained during oxidative phosphorylation [41]. A549 monolayers, grown in 96 well plates, were treated with 100 μg mL^{-1} of v- and ox-nPS/mPS suspensions for 24 h. After incubation at 37°C and washing in PBS to remove the non-internalised particles, cells were treated with the probe solution (10 μM final concentration) and incubated for 10 min at 37°C. Fluorimetric reading was carried out using a microplate reader (Tecan Italia) set to 535 and 595 nm as the excitation and emission wavelengths, respectively. In comparison to the control cells, the percentage changes of emission values were calculated for each sample.

2.7. Assessment of DNA damage by the comet assay

A549 cells treated for 24 h with virgin and oxidised mPS/nPS suspensions (100 μg mL^{-1}), were assessed for DNA integrity by using the alkaline version of the comet assay [42]. Tests were

 doi:10.20944/preprints202307.0678.v1

performed in duplicate on about 2 × 104 cells for each spot, and the electrophoresis was carried out for 30 min at 300 mA and 25 V (0.86 V cm^{-1}). The slides, stained with ethidium bromide (20 μg mL^{-1}), were imaged using a DMIRB fluorescence microscope (Leica Microsystems), equipped with a digital camera (Power Shot S50; Canon, Milan, Italy), at 400× total magnification. Samples were run in duplicate, and images of 100 cells per slide were acquired randomly and analysed by using the Comet Assay Software Project (CASP) software. %TDNA (i.e., %DNA in the tail) was considered the parameter of DNA damage.

2.8. Statistical analyses

All data are presented as the mean ± standard error (SE) based on at least three independent experiments. Analyses were performed using the Statistica programme (version10). Lilliefors and Shapiro–Wilk normality tests were used to assess data distribution patterns. The relationships between different parameters were assessed by using the Pearson correlation coefficient while the t Test was used to assess the differences between samples. Significance was accepted at $P < 0.05$.

3. Results

3.1. Cellular uptakes of mPS/nPS

To spectrofluorimetrically quantify the uptake of nPS-FITC/mPS-FITC in A549 cells, we generated a time course of emission values. Preliminary abiotic tests showed that the emission values (expressed in arbitrary fluorescence units [AFU]) in the experimental conditions were 97.13 and 72.45 for 1 μg of mPS and nPS, respectively. On this basis, in the range of 1.25–20 μg/well, we calculated the internalised amount (μg) at different times. The kinetics of nPS/mPS uptake indicated that internalisation was extremely fast. After 1h, at the lowest dose to which the cells were exposed, 20.8% and the 21.8% of the amount of nPS and mPS respectively, was internalised.

The results in Figure 1A are expressed as internalised amounts (μg/well) of nPS/mPS and clearly highlight the significant dose-effect correlation for both sizes of plastic particles (Pearson correlation coefficient [r] > 0.99). On the other hand, nPS and mPS showed distinct trends as a function of the exposure time (Figure 1B and 1C). The amounts of internalised mPS decreased as the exposure time increased for all tested doses; the percentage decrease (Δ%) was between 20% (at the lower doses 1.25–2.5 μg/well) and 30% (at the higher doses 5–20 μg/well). For nPS, this trend was observed only at the higher exposure doses (Δ% >30), while the uptake at lower doses increased by an average of 20% during the entire exposure period.

Preprints (www.preprints.org) | NOT PEER-REVIEWED | Posted: 11 July 2023 doi:10.20944/preprints202307.0678.v1

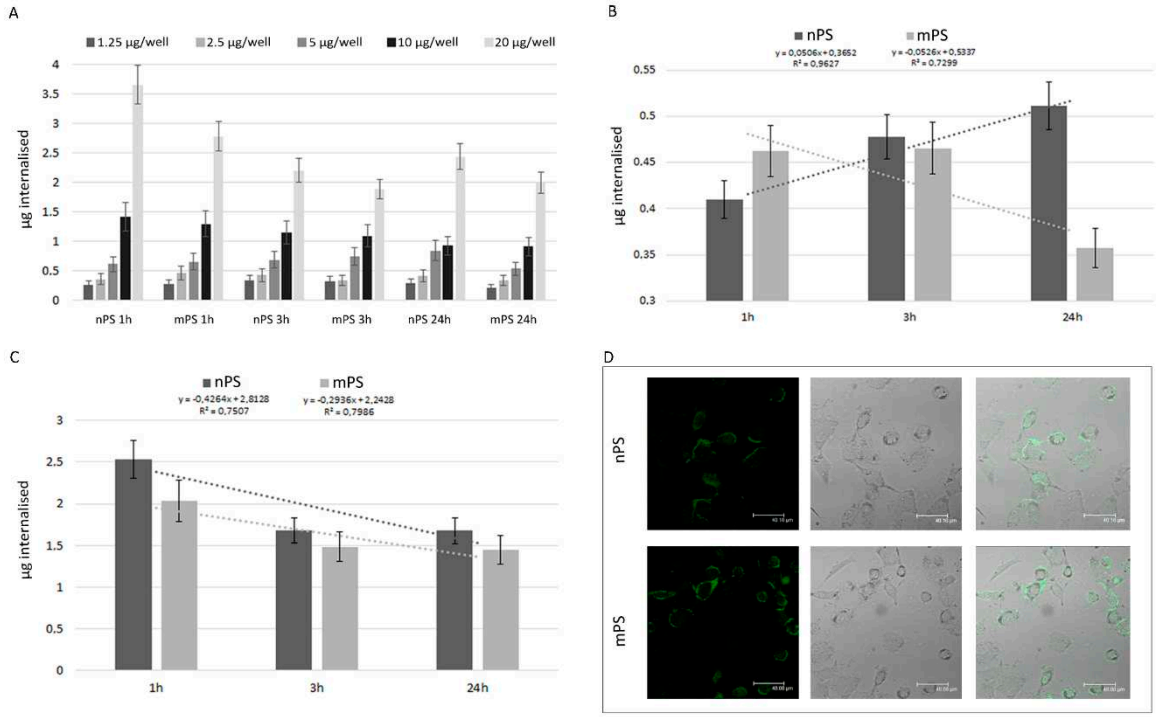

Figure 1. Cellular uptakes of mPS/nPS. A) Time course of spectrofluorimetric measurements of internalised µg of nPS-FITC/mPS-FITC in A549 cells treated in the range 1.25-20 µg/well. Highly significant dose-effect correlation for both sizes of plastic particles was observed ($P < 0.01$ to Pearson test). B, C) Trends of nPS-FITC/mPS-FITC uptake as a function of the exposure time in A549 cells exposed in the range of 1.25-2.5 µg/well (B) and in the range 5-20 µg/well (C). nPS-FITC/mPS-FITC uptake showed distinct trends at the lower doses. In B and C are reported the average values of internalised µg in cells treated with 1.25-2.5 and 5-20 µg/well of nPS-FITC/mPS-FITC. D) CLSM images of nPS-FITC/mPS-FITC internalisation in A549 semiconfluent monolayers treated for 1h at the dose corresponding to 10 µg/well. The cells exposed to mPS or nPS exhibited fair cytoplasmatic fluorescence, which was more intense in mPS-FITC-treated cells. In contrast microscopy image of these latter cells, intracytoplasmic aggregates of mPS were clearly visible.

Considering the PS density and the size of the particles, we calculated the total number of internalised particles: ~200 mPS and 200,000 nPS per µg internalised. The markedly higher number of internalised nPS highlights the greater surface area developed by the last ones. Because the experiments were performed in 96-well microplates with an average of 4 × 104 cells/well, regardless of the particle size, the uptake was in the range of 5.1–91.2 pg/cell.

CLSM confirmed the data and showed that the cells exposed to mPS/nPS exhibited fair cytoplasmatic fluorescence, which was clearly more intense in cells treated with the more fluorescent mPS (Figure 1D).

3.2. Assessment of the acidic compartment

Employing the metachromatic fluorophore AO, the microscopic analyses of the endocytic apparatus in cells treated with v-nPS/mPS for 3h highlighted a very bulky acidic compartment made up of numerous red organelles, clearly showing the consistent internalisation of both particles and, at the same time, the integrity of mature endosomes that almost completely occupied the perinuclear cytosol (Figure 2 A,B).

Preprints (www.preprints.org) | NOT PEER-REVIEWED | Posted: 11 July 2023 doi:10.20944/preprints202307.0678.v1

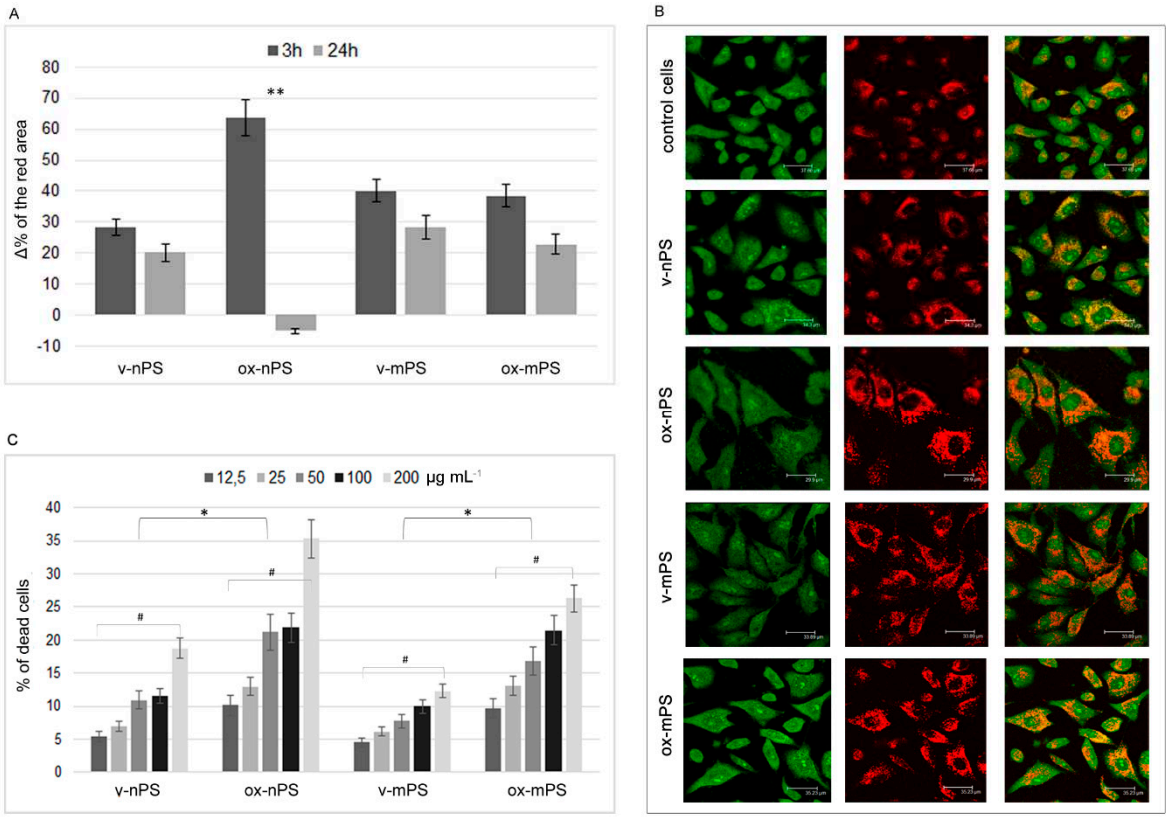

Figure 2. Changes in acidic compartment and cytotoxicity v- and ox- nPS/mPS-induced. A) The acidic compartment was assessed by employing metachromatic fluorophore AO which gives red color when, due to the lower pH values, the dye builds up. The graph (A) reports Δ% of the area emitting red fluorescence in exposed cells in comparison to control cells. The experiments were performed in semi-confluent A549 monolayers grown in chamber slides and treated for 3 and 24h at 37 °C with 100 μg mL-1 of v- and ox- mPS/nPS suspensions. A significant difference between 3 and 24h was observed for ox-nPS (P< 0.01 to t-test). B) Representative CLSM images in control and exposed cells (3h). A549 cells exposed to v- and ox- mPS/nPS suspensions showed an acidic compartment very bulky and made up of numerous red organelles that, particularly for ox-nPS, almost completely occupied the perinuclear cytosol. C) Results of MTT assay in A549 treated for 24 h in the range 12.5-200 μg mL-1, corresponding to 2.3 × 102–3.68 × 103 particles/well and 2.3 105–3.68 × 106 particles/well for mPS and nPS respectively. In comparison to the virgin nPS/mPS, the percentages of dead cells were significantly higher in ox-nPS and mPS (* P<0.05 to t-test). For all plastic particles the decrease of cell viability was positively related to the exposure dose (# P < 0.01 to Pearson test). Compared to mPS, nPS showed a moderately higher cytotoxic effect.

Compared to control cells, in the v-nPS/mPS-treated cells the Δ% of the area which emitted red fluorescence was 28.3 and 40.1, respectively, on average. In contrast to mPS, for which the values of v- and ox- were superimposable, a significant increase in the phagosomal compartment was observed in cells treated with ox-nPS (Δ% 65.5). Further changes in the endocytic apparatus were observed after 24 h when, in the cells treated with both v-nPS and v- and ox-mPS, a moderate reduction in the area of the acidic compartment was observed. This, underlining a possible spill from endocytic apparatus, more evident in cells treated with ox-nPS in which acidic organelles were also less developed than the control cells (Δ% -5.1) and the differences compared to 3h were highly significant (P < 0.01).

3.3. Cytotoxicity nPS/mPS-induced

We evaluated cytotoxicity in our cell model by using the MTT assay. The tested doses ranged from 12.5 to 200 μg mL^{-1}, corresponding to 2.3 × 10^2–3.68 × 10^3 particles/well and 2.3 10^5–3.68 × 10^6

 doi:10.20944/preprints202307.0678.v1

particles/well for mPS and nPS, respectively, with an exposure time of 24 h. Both virgin nPS and mPS had a moderate cytotoxic effect. Up to 200 μg mL^{-1}, cell viability was >80% and, at the lowest exposure dose, cell viability was only about 5% lower than the control cells (Figure 2C). Unlike virgins, a more marked cytotoxicity was elicited by oxidised particles. In comparison to the virgin nPS/mPS, the percentage of dead cells was 1.9-fold and more than double that in cells treated with ox-nPS and mPS, respectively ($P<0.05$). For all plastic particles, the decrease in cell viability was positively related to the exposure dose. For v- and ox-nPS, the percentage of dead cells ranged between 5.4 and 18.8 and between 10.1and 35.3, respectively ($P < 0.01$). For mPS, these percentages ranged from 4.5 to 12.3 and from 9.7 to 26.3, respectively ($P < 0.01$), underlining the moderately higher cytotoxic effect of nanosized particles.

3.4. ROS production

Figure 3A and B report the time course (0.5–24 h) of ROS production in A549 cells treated with v- and ox-nPS/mPS in the range 25–200 μg mL^{-1}. Similar to the kinetic uptake data, ROS overproduction was very fast and already evident after 0.5 h, especially for ox-nPS/mPS. Over time, ROS levels progressively increased, and r coefficients to the Pearson test were always >0.95 and similar to those calculated for the positive control (H_2O_2 300 μM). In the interval of 0.5–24h, DCF emission values increased on average by 15-fold for nPS and 17-fold for mPS, while no dose effect was observed for virgin nPS/mPS. The pro-oxidant effect of v-mPS was significantly higher, with ROS values which were double those of the v-nPS on average ($P < 0.05$) and only 20% lower than positive control. Compared to v-nPS/mPS, a further increase in intracellular ROS was observed in cells treated with oxidised particles. However, the increase was surprisingly smaller and equal to 40% for ox-nPS (P n.s). Conversely, ROS production induced by the ox-mPS was significantly increased in comparison to the virgin ones and the emission values of the probe were more than double ($P< 0.05$), confirming size-dependent differences.

Moreover, ROS overproduction induced by ox-mPS was positively related to doses ($P < 0.01$) and the probe emission values were double compared to the positive control already at 50 μg mL^{-1} (Figure 3B).

CLSM observations of the semiconfluent monolayers of v- and ox-nPS/mPS-treated cells (100 μg mL^{-1}) for 3 h confirmed the results (Figure 3C), highlighting diffuse green cytosolic fluorescence, which was more intense in mPS-treated cells. Moreover, as shown by magnification of phase contrast micrographs, intracellular clusters of particles are clearly visible in the mPS-treated cells (Figure 3D).

3.5. Mitochondrial impairment

Transmembrane potential ($\Delta\Psi m$) was detected to assess mitochondrial dysfunction induced by v- and ox-nPS/mPS. The experiments (Figure 4 A) highlighted a moderate decrease in nPS treated cells (%Δ 16 vs. control cells), without differences between v- and ox-nPS/mPS. Almost the same decrease was recorded in cells treated with ox-mPS. Instead, the virgin counterpart of these micro-sized particles did not alter mitochondrial function (%Δ -5 vs. control cells), clearly highlighting that ROS overproduction v-mPS-induced was directly attributable to the particles and not secondary to mitochondrial dysfunction.

Preprints (www.preprints.org) | NOT PEER-REVIEWED | Posted: 11 July 2023 doi:10.20944/preprints202307.0678.v1

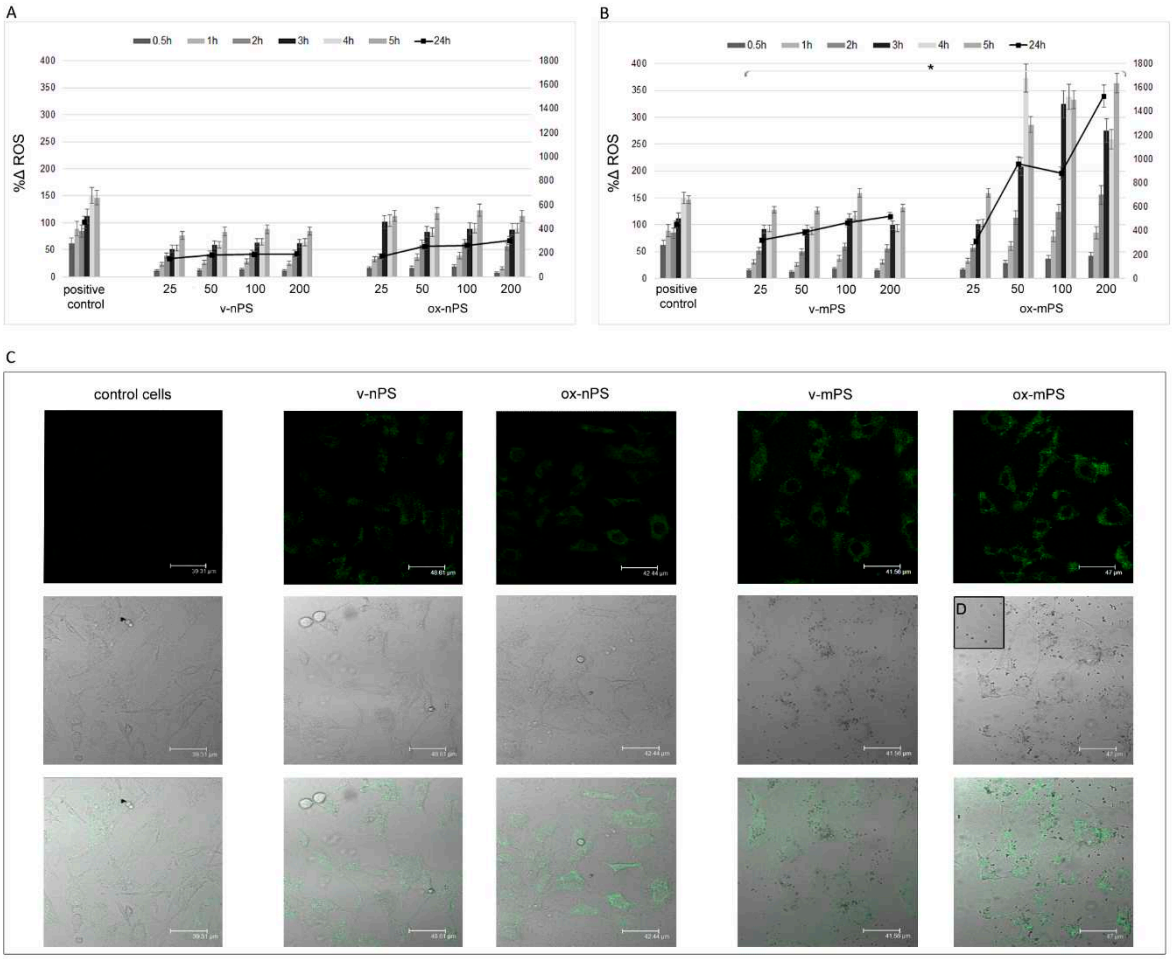

Figure 3. ROS overproduction v- and ox- nPS/mPS-induced. A and B) Time courses (0.5–24 h) of ROS in A549 cells treated with nPS and mPS respectively in the range of 25–200 μg mL-1. H2O2 (300 μM) was used as positive control and the values are reported as %Δ relative to control cells. The two scales on the y axis show the values recorded in the interval 0.5-5h on the left and those recorded at 24h on the right. For v- and ox- nPS/mPS, exposure time and ROS values were always significant related ($r > 0.95$; $P < 0.01$ to Pearson test). No dose effect was observed for v- nPS/mPS and for ox-nPS, conversely, ROS overproduction was positively related to doses ($P < 0.01$) for ox-mPS. Compared to v-nPS, significantly higher ROS values were observed for v-mPS ($P < 0.05$ to t-test). No significant differences were observed between v- and ox- nPS while significantly higher was the pro-oxidant effect of ox-mPS compared to v-mPS (*$P < 0.05$). C) CLSM images of the semiconfluent monolayers exposed to v- and ox- nPS/mPS- cells (100 μg mL-1) for 3 h and treated with DCF-DA probe. A diffuse green cytosolic fluorescence, more intense in ox-mPS-treated cells is shown. Moreover, as shown by D) magnification of phase contrast micrograph; intracellular clusters of particles are clearly visible in the mPS-treated cells.

Preprints (www.preprints.org) | NOT PEER-REVIEWED | Posted: 11 July 2023 doi:10.20944/preprints202307.0678.v1

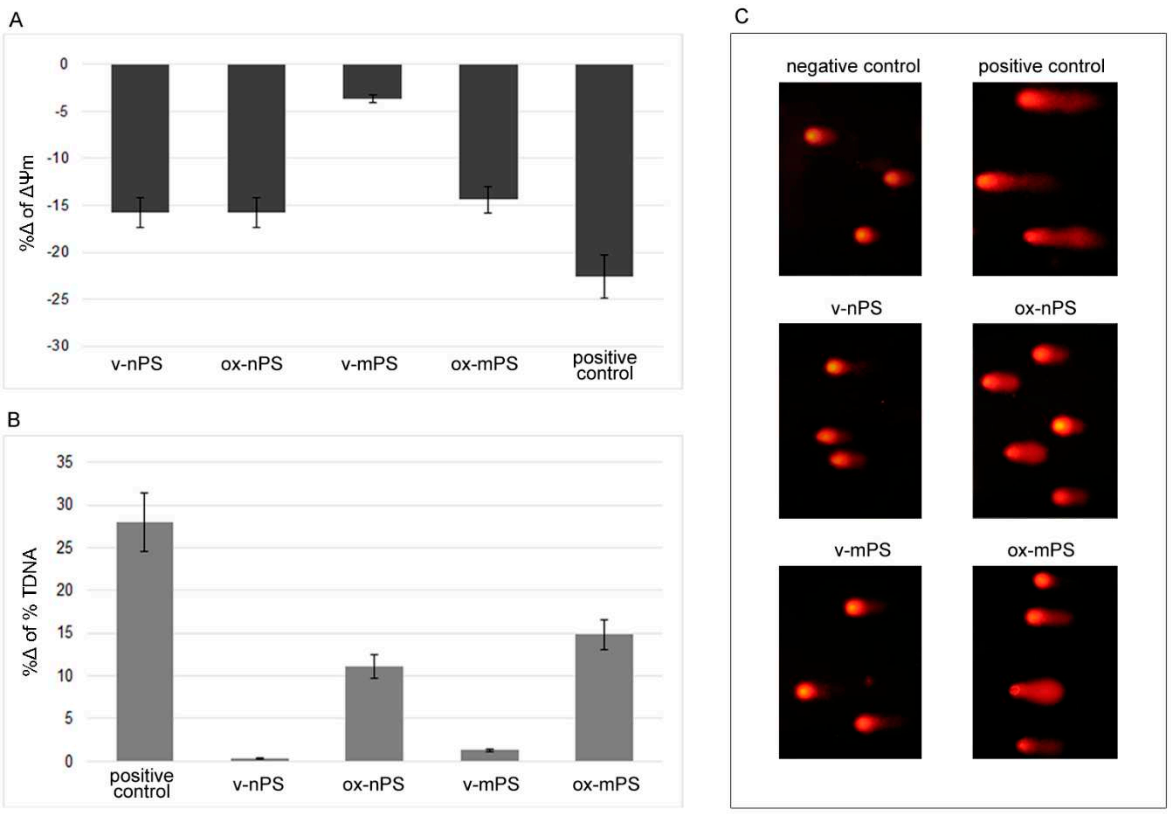

Figure 4. Mitochondrial impairment and DNA damage induced by v- and ox- nPS/mPS. A) %Δ of transmembrane potential (ΔΨm) measured spectrophotometrically by the employment of R123. Conversely to v-mPS, both v- and ox- nPS and ox-mPS caused a moderate mitochondrial impairment (%Δ 16 vs. control cells). B) Results expressed as %Δ of % TDNA to comet assay. The test was performed after overnight exposure to 100 μg mL^{-1} suspensions of v- and ox- nPS/mPS. H2O2 (300 μM) was used as positive control. Unlike v- nPS/mPS, the ones oxidised caused a moderate increase of DNA damage. C) Representative images of comet assay that was replicated three times with similar results. Compared to v- nPS/mPS treated cells, higher level of DNA damage is observed in ox-nPS/mPS treated cells.

3.6. Assessment of DNA damage by the comet assay

The genotoxicity of v- and ox-nPS/mPS was assessed by the comet assay performed after overnight exposure to 100 μg mL^{-1} suspensions. H_2O_2-treated cells (300 μM) served as the positive control. In our cell model, v-nPS/mPS did not cause DNA damage and the %TDNA values almost completely overlapped with the control cells (Figure 4 B and C). Conversely, both the oxidised particles were genotoxic and, compared to positive control, the %TDNA values were only 15% (nPS) and 10% (mPS) lower.

The results were consistent with ROS overproduction and highlight the oxidative DNA damage induced by exposure to oxidised nPS/mPS.

4. Discussion

The potential adverse health effects of breathable micro- and nanoplastics in humans are still poorly studied, despite the increasing quantities of airborne micro- and nanoplastics that can be found in the ambient air and, above all, in indoor environments. Several factors contribute to make plastic air pollution a threat for human health. These include both the features of micro- and nanoplastics and the anatomical and physiological characteristics of humans. As reported in the introduction, the progressive fragmentation of plastics and their low density favour their long stay in the air (fly particles). Other intrinsic features of the plastic particles such as hydrophobicity favour a closer interaction with cell membranes, inducing higher translocation rates [10].

Regarding humans, we must consider how the defence mechanisms of the respiratory system are undoubtedly less efficient against microparticles (≤2.5 μm) and, above all, nanoparticles (≤0.1 μm). In particular, while microparticles are phagocytosed by alveolar macrophages, a process which is much slower than mucociliary clearance and able to trigger the inflammatory cascade, nanoparticles may bypass macrophage clearance. To maximise gas exchange, the alveolar epithelium is extremely extended (about 140 m^2), and the alveolar-capillary barrier is particularly thin (<1 μm), which greatly favours the ability of nanoparticles to cross it and enter the bloodstream. Moreover, considering the volumes of air breathed daily (always >10 m^3 in adults), even a reduced presence of airborne micro- and nanoplastics (a single particle L^{-1} corresponds to 10,000 respired particles) would cause their accumulation both in the lungs and, by bloodstream, in other organs triggering pathogenic processes.

Our in vitro study improves knowledge on the mechanisms that regulate the biological effects of inhaled airborne micro- and nanoplastics, also considering the possible differences in the effects attributable to the surface changes of the particles due to oxidative processes, undergone during their environmental stay. As previously reported [37], the "artificial aging" used by us significantly increased the presence of carboxyl, alkoxyl and hydroxyl groups on their surface, simulating the photoaging, endured by the particles once released into the environment [43]. The increase in oxygen-containing groups after the oxidative process was confirmed by Fourier-Transform Infrared (FT-IR) spectrometry, dynamic light-scattering (DLS), scanning electron microscopy (SEM) and UV-Vis spectrophotometry [37], which coincided with that which was reported by Biale et al. (2021) [44], showing surface-limited formation of oxidised aromatic structures in PS particles without any involvement of the overall polymer mass. As assumed, the presence of oxygen-containing groups on the particle surface increased the reactivity and our results highlight the greater damage induced by the oxidised particles compared to the virgin ones, confirming the results of several studies [45–48].

By using homemade FITC-loaded nPS/mPS, we quantified the uptake and highlighted the speed at which both nPS and mPS were internalised. The volumes of air breathed and the observed internalisation rate, equal to approximately one fifth at low exposure doses, clearly underscore the potential impact of these emergent pollutants on human health. Similar to that which has been demonstrated for other particles [30], hydrophobicity favours the close interaction between micro- and nanoparticles and cell membranes, justifying both the speed of the process and the yield, as confirmed by the internalised doses, which ranged from 5.1 to 91.19 pg/cell. For both mPS and nPS, the process was significantly dose dependent, while only the internalisation of nPS at low doses was time-dependent.

Despite endocytosis is the main pathway of particle internalisation in all cells, we cannot exclude the possibility that nanoparticles can cross cell membranes via the energy-independent diffusion process. Diffusion is gradient-dependent and, albeit partially, is counteracted by the frictional coefficient of the particle that is in turn related to both the medium viscosity and the interactions between particles and macromolecules diluted in the solvent [49]. In particular, a diffusion process could be involved in the internalisation of plastic fibres that, due to their morphological parameters (i.e. the high length-to-diameter ratio), could efficiently penetrate biological membranes (needle-like crossing) [31]. Considering energy-dependent endocytosis, our cell models allowed us to verify internalisation in epithelial alveolar cells (pinocytosis) which involves actin polymerisation. Therefore, the process requires GTPase activity, and can be receptor-mediated (clathrin-dependent endocytosis or caveola-mediated endocytosis) [50]. The role of the endocytosis pathway had been confirmed in intestinal cells by using inhibitors of caveola-mediated and clathrin-mediated endocytosis, such as nystatin and chlorpromazine, respectively [51]. The same authors assessed the involvement of the cytoskeleton in uptake by measuring the actin levels, which were significantly higher in exposed cells. More recently, similar results were reported by Bonamoni et al. (2022) [52] on normal human intestinal cells (CCD-18Co) by using several inhibitors of endocytosis, such as Cytochalasin D and Genistein.

After membrane invagination, the particles are internalised in early endosomes, which merge with lysosomes to form endolysosomes (late endosomes); our results revealed the fast load (i.e. 3 h)

 doi:10.20944/preprints202307.0678.v1

of v- and ox-nPS/mPS in the acidic compartment, highlighted by the enlargement of endolysosomes. Extending observation times, the reduction of the acid compartment, particularly evident for ox-nPS, could be attributed to endolysosomal permeabilization, producing irreversible cytoplasmic acidification, enzymolysis and apoptosis (i.e., the Trojan horse effect) [34]. Excluding ox-nPS, the moderate cytotoxicity observed leads us to believe that a limited number of cells are involved in this effect. Conversely, the endolysosomal permeabilisation induced by ox-nPS was more marked, as confirmed by the higher percentage of dead cells recorded by the MTT test.

Despite the massive seizure in endocytic apparatus, a share of nPS/mPS randomly localises in the cell cytoplasm, causing the observed oxidative damage. We have reported similar results in HT-29 cells exposed to 3 and 10 μm PS particles [17] and similar results were obtained in Caco-2 cells [53].

For both nPS and mPS, the cellular-induced redox imbalance was time-dependent and higher in cells treated with oxidised mPS, confirming their intracellular bioavailability and the most powerful pro-oxidant effect of aged particles. Surprisingly, the redox imbalance of aged particles was more evident for mPS, despite the higher surface/mass ratio of the nPS, which notably increases reactivity [32]. This is conceivably imputable to the higher cytotoxicity elicited by ox-nPS that, causing the detachment of a large number of cells with internalised nPS, did not allow us to assess oxidative damage in its entirety.

The most powerful pro-oxidant effect of aged particles was highlighted by the results of the comet assay and mitochondrial transmembrane potential and, unlike the virgin counterpart, oxidised nPS/mPS was able to cause DNA damage and mitochondrial dysfunction.

Since oxidation is the most important degradation process to which plastics undergo during their aging in the environment, our results highlight in a more realistic way the potential health risk of the general population, mainly exposed to aged nPS/mPS. downsizing the value of the first in vitro studies almost always performed using virgin micro and nano polystyrene particles. However, it should be emphasised that nPS impaired mitochondrial function, regardless of whether it was virgin or oxidised. The decreases in transmembrane potential after exposure to v- and ox-nPS confirmed the results of Wu et al. (2019) [53] who observed transmembrane depolarisation in Caco-2 cells exposed to nanoplastics. In addition to nPS, ox-mPS also decreased transmembrane potential, confirming that mitochondrial impairment, by triggering a vicious circle, further contributes to ROS overproduction, which was significantly increased in cells exposed to ox-mPS. Moreover, considering the key role played by mitochondria in triggering apoptosis [54], the observed mitochondrial impairment is certainly not to be underestimated in outlining the pathogenetic mechanism of these emergent airborne pollutants.

5. Conclusions

Overall, our results highlight the potential negative effects of the respirable fraction of plastic particles on human health. These airborne particles, remaining in the environment for relatively prolonged times, undergo numerous degradation processes, including photochemical ones that cause oxidation, increasing their reactivity. Simulating the photoaging process and comparing the effects induced by oxidised nPS/mPS to those of virgins, we clearly demonstrated the greatest damage elicited by the former, underlining the importance of performing the risk assessment using environmental aged particles. Although the effects induced by these airborne pollutants are much less powerful than those of other airborne particles (combustion by-products, metals, engineered nanoparticles, etc.), their potential impact on human health cannot be excluded, especially if urgent action is not taken to limit their presence in the environment, significantly increased also due to SARS-CoV-2 pandemic.

Author Contributions: Conceptualization, A.D.P.; methodology, G.V., A.L. and C.C.; formal analysis, G.V., A.L. and A.F; data curation, A.D.P. and D.I.; writing—original draft preparation, A.D.P. All authors have read and agreed to the published version of the manuscript.

Funding: This research received no external funding.

Institutional Review Board Statement: Not applicable.

Informed Consent Statement: Not applicable.

Acknowledgments: The authors acknowledge support from the University of Messina through the APC initiative.

Conflicts of Interest: The authors declare no conflict of interest.

References

1. Li, W.C.; Tse, H.F.; Fok, L. Plastic waste in the marine environment: a review of sources, occurrence and effects. *Sci. Total. Environ*. **2016**, *566-567*, 333-349.
2. Domínguez-Jaimes, L.P.; Cedillo-González, E.I.; Luévano-Hipólito, E.; Acuña-Bedoya, J. D.; Hernández-López, J. M. Degradation of primary nanoplastics by photocatalysis using different anodized TiO2 structures. *J. Hazard. Mater.* **2021**, *413*, 125452.
3. Hirt, N.; Body-Malapel, M. Immunotoxicity and intestinal effects of nano- and microplastics: a review of the literature. *Part. Fibre Toxicol.* **2020**, *17*, 57.
4. Prata, J.C.; Da Costa, J.P.; Lopes, I.; Duarte, A.C.; Rocha-Santos, T. Environmental exposure to microplastics: An overview on possible human health effects. *Sci. Total. Environ.* **2020**, *702*, 134455.
5. Najahi, H.; Alessio, N.; Squillaro, T.; Conti G.O.; Ferrante, M.; Di Bernardo, G.; Galderisi, U.; Messaoudi, I.; Minucci, S.; Banni, M. Environmental microplastics (EMPs) exposure alter the differentiation potential of mesenchymal stromal cells. *Environ Res.* **2022**, *214*, 114088.
6. Li, Y.; Lu, Z.; Zheng, H.; Wang, J.; Chen, C. Microplastics in surface water and sediments of Chongming Island in the Yangtze Estuary, China. *Environ. Sci. Eur.* **2020**, *32*, 15.
7. Yang, L.; Zhang, Y.; Kang, S.; Wang, Z.; Wu, C. Microplastics in soil: A review on methods, occurrence, sources, and potential risk. *Sci. Total. Environ.* **2021**, *780*, 146546.
8. Alfaro-Núñez, A.; Astorga, D.; Cáceres-Farías, L.; Bastidas, L.; Soto Villegas, C.; Macay, K.C.; Christensen, J.H. Microplastic pollution in seawater and marine organisms across the Tropical Eastern Pacific and Galápagos. *Sci. Rep.* **2021**, *11*, 6424.
9. Pastorino, P.; Prearo, M.; Pizzul, E.; Elia, A.C.; Renzi, M.; Ginebreda, A.; Barceló, D. High-mountain lakes as indicators of microplastic pollution: current and future perspectives. *Water Emerg. Contam. Nanoplastics* **2022**, *1*, 3.
10. Facciolà, A.; Visalli, G.; Pruiti Ciarello, M.; Di Pietro, A. Newly Emerging Airborne Pollutants: Current Knowledge of Health Impact of Micro and Nanoplastics. *Int. J. Environ. Res. Public Health.* **2021**, *18*, 2997.
11. Lim, X. Microplastics are everywhere - but are they harmful? *Nature* **2021**, *593*, 22-25.
12. Saley, A.M.; Smart, A.C.; Bezerra, M.F.; Burnham, T.L.U.; Capece, L.R.; Lima, L.F.O.; Carsh, A.C.; Williams, S.L; Morgan, S.G. Microplastic accumulation and biomagnification in a coastal marine reserve situated in a sparsely populated area. *Mar. Pollut. Bull*. **2019**, *146*, 54-59.
13. Miller, M.E.; Hamann, M.; Kroon, F.J. Bioaccumulation and biomagnification of microplastics in marine organisms: A review and meta-analysis of current data. *PLoS ONE* **2020**, *15*, e0240792.
14. Dris, R.; Gasperi, J.; Mirande, C.; Mandin, C.; Guerrouache, M.; Langlois, V.; Tassin, B. A first overview of textile fibers, including microplastics, in indoor and outdoor environments. *Environ. Pollut.* **2017**, *221*, 453–458.
15. Campanale, C.; Massarelli C.; Savino I.; Locaputo, V.; Uricchio, V.F. A Detailed Review Study on Potential Effects of Microplastics and Additives of Concern on Human Health. *Int. J. Environ. Res. Public Health* **2020**, *17*, 1212.
16. Enyoh, C. E.; Shafea, L.; Verla, A. W.; Verla, E.N.; Qingyue, W.; Chowdhury, T.; Paredes, M. Microplastics Exposure Routes and Toxicity Studies to Ecosystems: An Overview. *Environ Anal Health Toxicol.* **2020**, *35*, e2020004.
17. Visalli, G.; Facciolà, A.; Pruiti Ciarello, M.; De Marco, G.; Maisano, M.; Di Pietro, A. Acute and Sub-Chronic Effects of Microplastics (3 and 10 μm) on the Human Intestinal Cells HT-29. *Int. J. Environ. Res. Public Health.* **2021**, *18*, 5833.
18. Zarus, G.M.; Muianga, C.; Hunter, C.M.; Pappas, R.S. A review of data for quantifying human exposures to micro and nanoplastics and potential health risks. *Sci. Total. Environ* **2021**, *756*, 144010.

19. Bredeck, G.; Halamoda-Kenzaoui, B.; Bogni, A.; Bogni, A.; Lipsa, D.; Bremer-Hoffmann, S. Tiered testing of micro- and nanoplastics using intestinal in vitro models to support hazard assessments. *Environ. Int.* **2022**, *158*, 106921.
20. Schwabl, P.; Köppel, S.; Königshofer, P.; Bucsics, T.; Trauner, M.; Reiberger, T.; Liebmann, B. Detection of Various Microplastics in Human Stool: A Prospective Case Series. *Ann. Intern. Med.* **2019**, *171*, 453-457.
21. Ibrahim, Y.S.; Tuan Anuar, S.; Azmi, A.A.; Wan Mohd Khalik, W.M.A.; Lehata, S.; Hamzah, S.R.; Ismail, D.; Ma, Z.F.; Dzulkarnaen, A.; Zakaria, Z.; et al. Detection of microplastics in human colectomy specimens. *JGH Open* **2020**, *5*, 116-121.
22. Amato-Lourenço, L.F.; Carvalho-Oliveira, R.; Júnior, G.R.; Dos Santos Galvão, L.; Ando, R.A.; Mauad, T. Presence of airborne microplastics in human lung tissue. *J. Hazard Mater.* **2021**, *416*, 126124.
23. Braun, T.; Ehrlich, L.; Henrich, W.; Koeppel, S.; Lomako, I.; Schwabl, P.; Liebmann, B. Detection of Microplastic in Human Placenta and Meconium in a Clinical Setting. *Pharmaceutics* **2021**, *13*, 921.
24. Ragusa, A.; Svelato, A.; Santacroce, C.; Catalano, P.; Notarstefano, V.; Carnevali, O.; Papa, F.; Rongioletti, M.C.A.; Baiocco, F.; Draghi, S.; et al. Plasticenta: First evidence of microplastics in human placenta. *Environ. Int.* **2021**, *146*, 106274.
25. Prata, J.C. Airborne microplastics: Consequences to human health? *Environ. Pollut.* **2018**, *234*, 115-126.
26. Chen, G.; Feng, Q.; Wang, J. Mini-review of microplastics in the atmosphere and their risks to humans. *Sci Total Environ.* **2020**, *703*, 135504.
27. Liao, Z.; Ji, X.; Ma, Y.; Lv, B.; Huang, W.; Zhu, X.; Fang, M.; Wang, Q.; Wang, X.; Dahlgren, R.; et al. Airborne microplastics in indoor and outdoor environments of a coastal city in Eastern China. *J Hazard Mater.* **2021**, *417*, 126007.
28. Evangeliou, N.; Grythe, H.; Klimont, Z.; Heyes, C.; Eckhardt, S.; Lopez-Aparicio, S.; Stohl, A. Atmospheric transport is a major pathway of microplastics to remote regions. *Nat. Commun.* **2020**, *11*, 1 – 11.
29. Xumiao, L.; Prata, J.C.; Alves, J.R.; Duarte, A.C.; Rocha-Santos, T.; Cerqueira, M. Airborne microplastics and fibers in indoor residential environments in Aveiro, Portugal. *Environ. Adv.* **2021**, *6*, 100134.
30. Visalli, G.; Currò, M.; Iannazzo, D.; Pistone, A.; Pruiti Ciarello, M.; Acri, G.; Testagrossa, B.; Bertuccio, M.P.; Squeri, R.; Di Pietro, A. In vitro assessment of neurotoxicity and neuroinflammation of homemade MWCNTs. *Environ. Toxicol. Pharmacol.* **2017**, *56*, 121-128.
31. Facciolà, A.; Visalli, G.; La Maestra, S.; Ceccarelli, M.; D'Aleo, F.; Nunnari, G.; Pellicanò, G. F.; Di Pietro, A. Carbon nanotubes and central nervous system: Environmental risks, toxicological aspects and future perspectives. *Environ. Toxicol. Pharmacol.* **2019**, *65*, 23-30.
32. Visalli, G.; Facciolà, A.; Currò, M.; Laganà, P.; La Fauci, V.; Iannazzo, D.; Pistone, A.; Di Pietro, A. Mitochondrial Impairment Induced by Sub-Chronic Exposure to Multi-Walled Carbon Nanotubes. *Int. J. Environ. Res. Public Health* **2019**, *16*, 792.
33. Puisney, C.; Baeza-Squiban, A.; Boland, S. Mechanisms of Uptake and Translocation of Nanomaterials in the Lung. *Adv. Exp. Med. Biol.* **2018**, *1048*, 21-36.
34. Trovato, M.C.; Andronico, D.; Sciacchitano, S.; Ruggeri, R.M.; Picerno, I.; Di Pietro, A.; Visalli, G. Nanostructures: Between natural environment and medical practice. *Rev. Environ. Health.* **2018**, *33*, 295–307.
35. Hu, M.; Palić, D. Micro- and nano-plastics activation of oxidative and inflammatory adverse outcome pathways. *Redox Biol.* **2020**, *37*, 101620.
36. Mielczarski, J.A.; Jeyachandran, Y.L.; Mielczarski, E.; Rai, B. Modification of polystyrene surface in aqueous solutions. *J. Colloid Interface Sci.* **2011**, *362*, 532-539.
37. Visalli, G.; Laganà, A.; Facciolà, A.; Iaconis, A.; Curcio, J.; Pollino, S.; Celesti, C.; Scalese, S.; Libertino, S.; Iannazzo, D.; et al. Enhancement of biological effects of oxidised nano- and microplastics in human professional phagocytes. *Environ Toxicol Pharmacol.* **2023**, *99*, 104086.
38. Ter Liu, N.; Tang, M.; Ding, J. The interaction between nanoparticles-protein corona complex and cells and its toxic effect on cells. *Chemosphere* **2020**, *245*, 125624.
39. Visalli, G.; Bertuccio, M.P.; Iannazzo, D.; Piperno. A.; Pistone, A.; Di Pietro, A. Toxicological assessment of multi-walled carbon nanotubes on A549 human lung epithelial cells. *Toxicol. In Vitro* **2015**, *29*, 352-362.
40. Micale, R.T.; La Maestra, S.; Di Pietro, A.; Visalli, G.; Baluce, B.; Balansky, R.; Steele, V.E.; De Flora, S. Oxidative stress in the lung of mice exposed to cigarette smoke either early in life or in adulthood. *Arch. Toxicol.* **2013**, *87*, 915-918.

41. Di Pietro, A.; Baluce, B.; Visalli, G.; La Maestra, S.; Micale, R.; Izzotti, A. Ex vivo study for the assessment of behavioral factor and gene polymorphisms in individual susceptibility to oxidative DNA damage metals-induced. *Int. J. Hyg. Environ. Health* **2011**, *214*, 210–218.
42. Visalli, G.; Baluce, B.; La Maestra, S.; Micale, R.T.; Cingano, L.; De Flora, S.; Di Pietro, A. Genotoxic damage in the oral mucosal cells of subjects carrying restorative dental fillings. *Arch. Toxicol.* **2013**, *87*, 2247-2248.
43. Zhang, X.; Xia, M.; Zhao, J.; Cao, Z.; Zou, W.; Zhou, Q. Photoaging enhanced the adverse effects of polyamide microplastics on the growth, intestinal health, and lipid absorption in developing zebrafish. *Environ. Int.* **2022**, *158*, 106922.
44. Biale, G.; La Nasa, J.; Mattonai, M.; Corti, A.; Vinciguerra, V.; Castelvetro, V.; Modugno, F.A. Systematic Study on the Degradation Products Generated from Artificially Aged Microplastics. *Polymers (Basel)* **2021**, *13*, 1997.
45. Zhu, K.; Jia, H.; Sun, Y.; Dai, Y.; Zhang, C.; Guo, X.; Wang, T.; Zhu, L. Enhanced cytotoxicity of photoaged phenol-formaldehyde resins microplastics: combined effects of environmentally persistent free radicals, reactive oxygen species, and conjugated carbonyls. *Environ. Int.* **2020**, *145*, 106137.
46. Shi, X.; Chen, Z.; Liu, X.; Wei, W.; Ni, B.J. The photochemical behaviors of microplastics through the lens of reactive oxygen species: Photolysis mechanisms and enhancing photo-transformation of pollutants. *Sci. Total Environ*. **2022**, *846*, 157498.
47. Völkl, M.; Jérôme, V.; Weig, A.; Jasinski, J.; Meides, N.; Strohriegl, P.; Scheibel, T.; Freitag, R. Pristine and artificially-aged polystyrene microplastic particles differ in regard to cellular response. *J. Hazard. Mater*. **2022**, *435*, 128955.
48. Yu, X.; Lang, M.; Huang, D.; Yang, C.; Ouyang, Z.; Guo, X. Photo-transformation of microplastics and its toxicity to Caco-2 cells. *Sci. Total Environ*. **2022**, 150954.
49. Visalli, G.; Facciolà, A.; Iannazzo, D.; Piperno, A.; Pistone, A.; Di Pietro, A. The role of the iron catalyst in the toxicity of multi-walled carbon nanotubes (MWCNTs). *J. Trace Elem. Med. Biol.* **2017**, *43*, 153-160.
50. Katayama, K.; Nomura, H.; Ogataa, H.; Eitoku, T. Diffusion coefficients for nanoparticles under flow and stop-flow conditions. *Phys. Chem. Chem. Phys.* **2009**, *11*, 10494-10499.
51. Varma, S.; Dey, S.; Palanisamy, D. Cellular Uptake Pathways of Nanoparticles: Process of Endocytosis and Factors Affecting their Fate. *Curr. Pharm. Biotechnol*. **2022**, *23*, 679-706.
52. Bonanomi, M.; Salmistraro, N.; Porro, D.; Pinsino, A.; Colangelo, A.M.; Gaglio, D. Polystyrene micro and nano-particles induce metabolic rewiring in normal human colon cells: A risk factor for human health. *Chemosphere*. **2022**, *303*, 134947.
53. Wu, B.; Wu, X.; Liu, S.; Wang, Z.; Chen, L. Size-dependent effects of polystyrene microplastics on cytotoxicity and efflux pump inhibition in human Caco-2 cells. *Chemosphere* **2019**, *221*, 333–341.
54. Visalli, G.; Baluce, B.; Bertuccio, M.; Picerno, I.; Di Pietro, A. Mitochondrial-mediated apoptosis pathway in alveolar epithelial cells exposed to the metals in combustion-generated particulate matter. *J. Toxicol. Environ. Health A*, **2015**, *78*, 697-709.